

Article

Medium-Range Order Resists Deformation in Metallic Liquids and Glasses

Takeshi Egami^{1,2,3,*} , Wojciech Dmowski¹ and Chae Woo Ryu⁴ 

¹ Shull-Wollan Center and Department of Materials Science and Engineering, University of Tennessee, Knoxville, TN 37996, USA

² Department of Physics and Astronomy, University of Tennessee, Knoxville, TN 37996, USA

³ Materials Sciences and Technology Division, Oak Ridge National Laboratory, Oak Ridge, TN 37831, USA

⁴ Department of Materials Science and Engineering, Hongik University, Seoul 04066, Republic of Korea

* Correspondence: egami@utk.edu

Abstract: In crystals, lattice defects, such as dislocations, control mechanical deformation. Similarly, it is widely believed that even in glasses and liquids some kinds of defects, strongly disordered regions, play a major role in deformation. To identify defects researchers focused on the nature of the short-range order (SRO) in the nearest neighbor cage of atoms. However, recent results by experiment, simulation and theory raise serious questions about this assumption. They suggest that the atomic medium-range order (MRO) provides resistance against flow at the atomic level. Because the MRO is a bulk property, it implies that defects play only a limited role. This new insight is supported by the density wave theory which shows that the MRO is driven by a top-down global force, rather than being a consequence of the SRO in the bottom-up manner, and the MRO provides stiffness to resist deformation. We briefly summarize the density wave theory, show that the MRO is related to ductility of metallic glasses, and discuss the implications on the role of the MRO in the atomic-level mechanism of deformation.

Keywords: metallic glass; medium-range-order; liquid viscosity; glass deformation



Citation: Egami, T.; Dmowski, W.; Ryu, C.W. Medium-Range Order Resists Deformation in Metallic Liquids and Glasses. *Metals* **2023**, *13*, 442. <https://doi.org/10.3390/met13030442>

Academic Editor: Sundeep Mukherjee

Received: 28 January 2023

Revised: 15 February 2023

Accepted: 19 February 2023

Published: 21 February 2023



Copyright: © 2023 by the authors. Licensee MDPI, Basel, Switzerland. This article is an open access article distributed under the terms and conditions of the Creative Commons Attribution (CC BY) license (<https://creativecommons.org/licenses/by/4.0/>).

1. Introduction

Elucidating the atomic structures of liquid and glass is a major challenge because of their strong disorder [1–3]. The conventional approach is to consider an atom and its nearest neighbor shell, choose some relatively stable configurations, such as icosahedral clusters, and to use them as building blocks to construct the entire structure [4–8]. This bottom-up approach, however, does not explain well why well-defined medium-range order (MRO) is widely observed in the structure even in chemically complex liquids and glasses [9–13]. The MRO is characterized by the exponential decay of the oscillations in the pair-distribution function (PDF), $g(r)$, beyond the first peak [14],

$$|g(r) - 1| \approx \frac{\exp(-r/\xi_s(T))}{r} \quad (1)$$

where $\xi_s(T)$ is the structural coherence length. The bottom-up approach also fails to explain the distinct behaviors of the MRO and the short-range order (SRO) represented by the first peak of the PDF which describes the distribution of near neighbor distances. For instance, in liquid the average nearest neighbor distance actually decreases with increasing temperature, whereas the distances to further neighbors increase [15,16]. Also, the MRO freezes at the glass transition temperature, T_g , whereas the SRO does not [17]. In the conventional bottom-up approach the MRO is just a consequence of the SRO, as described by the Ornstein-Zernike theory [14]. Then, both the SRO and the MRO should freeze simultaneously at T_g . The distinct behaviors of the MRO and the SRO reflect the fact that they are different in nature. The number of neighbors contributing to the first peak of

the PDF is of the order of 10, but the higher order peaks represent much larger numbers of atoms. Therefore, the SRO describes the atom-atom correlations, whereas the MRO represents the correlation between an atom and coarse-grained density fluctuations [18]. Therefore, it is possible that they are driven by different kinds of driving force.

Recently, we found that the MRO is driven by many-body forces in reciprocal space to form the density waves in liquid [19,20]. These forces are quite distinct from those in real space which promote formation of the local SRO. This result was obtained by the density wave theory with the pseudopotential for interatomic interaction. Here, we briefly summarize this theory and discuss its implications on the mechanical properties of liquid and glass. We focus mainly on metallic liquids and glasses which are simplest groups of liquid and glass.

2. Density Wave Theory

The traditional bottom-up approach may be appropriate in describing the crystal growth, but liquid does not form in such a way. To consider condensation from gas, it is better to start with a model of non-interacting particles and introduce interatomic interaction to all atoms at once, in a top-down approach. This is done best in reciprocal space, using the density wave theory. But the Fourier-transform of the interatomic potential is dominated by the strongly repulsive part of the potential, leading to nonsensical results. However, this is misleading, because the strongly repulsive part of the potential is irrelevant in evaluating the total potential energy. Precisely because of the repulsive part of the potential, atoms do not come very close to each other at temperatures we consider. Therefore, we only need a moderately repulsive potential, and we can safely ignore the strongly repulsive part of the potential. In other words, in terms of the potential energy landscape (PEL) [21,22], we should focus only on the accessible part of the PEL at temperatures we consider, instead of the entire PEL. Thus, we define the pseudopotential by

$$\phi(r) = \phi_{pp}(r) + \phi_R(r) \quad (2)$$

here $\phi(r)$ is the full potential, and $\phi_{pp}(r)$ is the “pseudopotential” in which the strongly repulsive part of $\phi(r)$ is removed and $\phi_{pp}(r) = \phi(r_c)$ is assumed for $r < r_c$, as in Figure 1 for the Lennard-Jones potential for argon [23]. The cutoff, r_c , is chosen such that the cutoff temperature, $k_B T_u = \phi(r_c)$ is well above the glass transition temperature and no pair of atoms is found at distances of $r < r_c$. The $\phi_R(r)$ is the strongly repulsive part of the potential below r_c . The total potential energy is given by,

$$U = U_{pp} + U_R \quad (3)$$

where

$$U_{pp} = \int \rho(\mathbf{r}) \rho^*(\mathbf{r}') \phi_{pp}(|\mathbf{r} - \mathbf{r}'|) d\mathbf{r} d\mathbf{r}' \quad (4)$$

$$U_R = \int \rho(\mathbf{r}) \rho^*(\mathbf{r}') \phi_R(|\mathbf{r} - \mathbf{r}'|) d\mathbf{r} d\mathbf{r}' = 0 \quad (5)$$

Note that $U_R = 0$, because no pair of atoms is found at distances of $r < r_c$. Therefore, in determining the structure we only need to minimize U_{pp} , not the total U .

Interestingly, it was found that the Fourier-transform of $\phi_{pp}(r)$, $\phi_{pp}(q)$, has a minimum at q_{min} , which is not far from the position of the first peak of the structure function determined by diffraction measurement, $S(q)$, $q_1 = 2.0^{-1}$ in this case, as shown in Figure 2. This is not an accident, and various potentials show similar results that q_{min} is close to q_1 [19,20]. It is long known that q_1 is related to the position of the first peak of the PDF, r_1 , by $r_1 \sim 5\pi/2q_1$ [9,20]. This is because $g(r)$ is related to $S(q)$ through [24],

$$g(r) = 1 + \frac{1}{2\pi^2 \rho_0} \int_0^\infty [S(q) - 1] \frac{\sin(qr)}{qr} q^2 dq \quad (6)$$

where ρ_0 is the atomic number density, and $\sin(x)/x$ has the first maximum near $x = 5\pi/2$. For the same reason $\phi_{pp}(q)$ has a minimum near q_1 , corresponding to the minimum in $\phi_{pp}(r)$ at $r = a$. It is also possible to explain this result in terms of the general scattering theory [25].

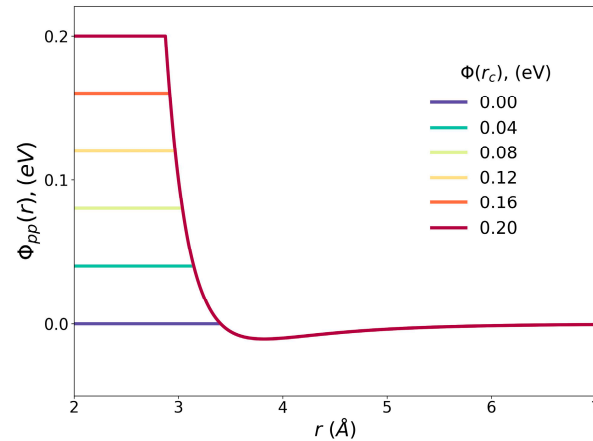


Figure 1. The pseudopotential of the Lennard-Jones potential with various cut-off levels.

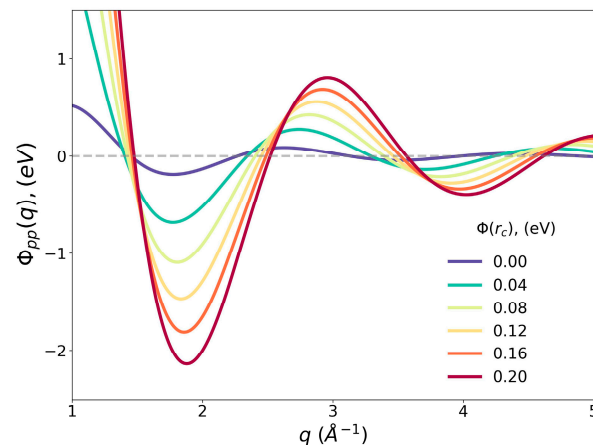


Figure 2. The Fourier transform of the pseudopotential of the Lennard-Jones potential, $\phi_{pp}(q)$, with various cut-off levels.

A minimum in $\phi_{pp}(q)$ drives the system to form a density wave with $q_{DW} \sim q_{min}$. Because liquid is macroscopically isotropic, the density waves are excited in all directions, so that the q_{DW} with a fixed length at $q_{DW} = |q_{DW}|$ forms a sphere. The density function of such a state is given by,

$$\rho(\mathbf{r}) = \rho_{DW}(\mathbf{r}) = \rho_0 + \int \rho(\mathbf{q}_{DW}) e^{i\mathbf{q}_{DW} \cdot \mathbf{r}} d\mathbf{q}_{DW} \quad (7)$$

where

$$\rho(\mathbf{q}_{DW}) = |\rho(\mathbf{q}_{DW})| e^{i\delta_{DW}(\mathbf{q}_{DW})} \quad (8)$$

The phase factor, $\delta_{DW}(\mathbf{q}_{DW})$, is added to avoid atom pileups. The phase factor varies strongly and nearly randomly for the q_{DW} vectors in different directions within the \mathbf{q} sphere. This state, the density wave (DW) state, has long-range periodic order without translational symmetry. Now, the structure function, $S(\mathbf{q})$, is related to $\rho(\mathbf{q})$, by

$$S(\mathbf{q}) = \frac{V}{\rho_0} |\rho(\mathbf{q})|^2 \quad (9)$$

where V is the system volume. Thus, $S(\mathbf{q})$ has a δ -function at $q_{DW} = |q_{DW}|$, and in three-dimensional q space q_{DW} s form a Bragg sphere. The PDF of the DW state is,

$$g_{DW}(r) = 1 + \frac{V^{\frac{2}{3}} q_{DW}^2}{\pi \rho_0^2} \langle |\rho(q_{DW})|^2 \rangle \frac{\sin q_{DW} r}{q_{DW} r} \quad (10)$$

characterized by the MRO-like oscillations. As the δ -function in $S(q)$ suggests this state has long-range atomic correlations, but because of the incoherent nature of the phase factors there is no macroscopic periodicity in the structure. Quasicrystal [26] was the first case of such a state with long-range order without periodicity, characterized by two base vectors in six-dimensions [27]. The DW state is defined by N vectors in N -dimensional reciprocal space, where N is the number of atoms in the system. Thus, the DW state is a crystal in N -dimensions, but there are a large number of ways to project this N -dimensional state to three-dimensional space. The projection is defined by sets of the phase factors and amplitudes, denoted by Λ [20]. This degeneracy becomes an issue in real glasses as discussed below.

In the conventional bottom-up approach we try to minimize the potential, $\phi(r)$, in real space starting with an atom at the center. This leads to better local packing, for instance by forming icosahedral clusters [4,6,7]. But, at the next step the existing cluster becomes a strong constraint [8], often expressed as geometrical frustration [5]. Our top-down approach is totally orthogonal; we start with the non-interacting gas state and introduce the interaction in reciprocal space. This top-down approach leads to the density wave state given by Equation (7).

3. Origin of the MRO

3.1. Structurally Coherent Ideal Glass State

The $\xi_s(T)$ follows the Curie-Weiss law in its temperature dependence,

$$\frac{\xi_s(T)}{a} = C \frac{T_g}{T - T_{IG}} \quad (T > T_g) \quad (11)$$

where a is the average near neighbor distance, T_g is the glass transition temperature and T_{IG} is the ideal glass temperature where $\xi_s(T)$ diverges in extrapolation [11]. We call this state the structurally coherent ideal glass (IG) state. This state cannot be physically reached because $\xi_s(T)$ freezes at T_g and becomes constant in the glassy state, and also because the value of T_{IG} is negative for all metallic liquids we studied. Nevertheless, this state is very useful as the reference state to discuss the origin of the MRO. The structure of the IG state can be estimated from the glass structure with a finite ξ_s . From Equation (1) we can write,

$$G(r) = 4\pi r \rho_0 [g(r) - 1] = G_0(r) \exp(-r/\xi_s(T)) \quad (12)$$

The state represented by

$$G_0(r) = G(r) \exp(r/\xi_s(T)) \quad (13)$$

is an imaginary state obtained by extrapolating $\xi_s(T)$ to infinity. This state approximately represents the IG state, if we assume only $\xi_s(T)$ changes with temperature. Indeed, the temperature dependence by Equation (11) is explained in terms of random local density fluctuations away from the IG state, justifying this assumption [28]. The state represented by $G_0(r)$ has no attenuation in the density waves, and thus $S(q)$ has a δ -function as the first peak, just as the DW state. However, the first peak of $g(r)$ of this state is taller than that of $g_{DW}(r)$, resulting in the oscillation at high q in $S(q)$ [11]. Thus, the IG state is very similar to the DW state, but it is slightly closer to the real glass state.

It was possible to create a model structure which approximately reproduces the $G_0(r)$. We obtained $G_0(r)$ from the $G(r)$ determined experimentally for Pd_{42.5}Ni_{7.5}Cu₃₀P₂₀ alloy liquid, and created a model by using the reverse Monte-Carlo (RMC) method [29] with a condition of some minimum atomic separation [11]. The PDF of the model shows the oscillations very similar to those in Equation (10). Visually the model appears totally random and liquid-like, even though it has positional correlation over long-range [11].

3.2. Compromise between DW State and the SRO

The SRO of the model defined by Equation (13) was found to be quite diverse and poorly ordered. For instance, the fraction of the icosahedral local order is only 0.7%, while the glass state obtained by molecular dynamics (MD) simulation with the same potential has the icosahedral local order population of nearly 10% [11]. Apparently, placing the priority on long-range order by assuming the density waves produced poor SRO. In other words, the top-down approach to minimize the potential energy in q space, resulting in the density wave state, is incompatible with the bottom-up approach to minimize the potential energy in real space to produce good SRO.

As shown in Figure 3 the MRO oscillation can be described well by

$$g(r) - 1 \approx A_{MRO} \frac{a}{r} \sin(Q_{MRO}r + \delta_{MRO}) \exp\left(-\frac{r}{\xi_s}\right), \quad r > r_{cutoff} \quad (14)$$

where A_{MRO} is the amplitude of the MRO oscillation, δ_{MRO} is the phase factor which is small, and r_{cutoff} is the position of the first minimum of the PDF beyond the first peak. Thus, the MRO oscillation is very similar to the PDF of the DW state except for the exponential attenuation. For this reason, we propose that the attenuation of the density waves by an exponential function is the origin of the MRO. To mitigate the conflict between the density wave state and the SRO, density waves are exponentially attenuated resulting in the MRO, given by Equation (14).

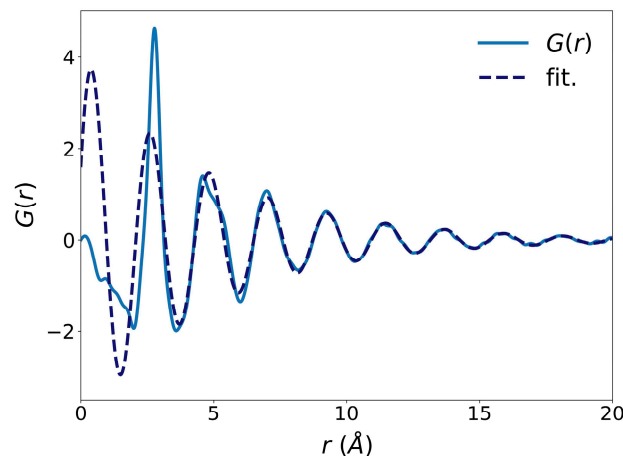


Figure 3. The $G(r)$ of $\text{Pd}_{42.5}\text{Ni}_{7.5}\text{Cu}_{30}\text{P}_{20}$ alloy liquid at $T = 573$ K (solid line) and the fit by Equation (14) (dashed line).

Then, in real glass the IG state by Equation (7) is limited to locality, of which size is defined by $\xi_s(T)$. As we noted above even though the DW state is a uniquely defined crystal in N -dimensions, there are a large number of ways to project it to three-dimensional space, defined by the sets of phase factors and amplitudes, Λ . So, the DW state associated with the local IG state changes with position and Λ varies in space as $\Lambda(r)$ [20]. The limited range of the DW order makes the first peak of $S(q)$ broader, with the width reciprocally proportional to ξ_s . In the case of pure exponential decay, the peak shape is Lorentzian. Indeed, glasses with long ξ_s have more Lorentzian first peak of $S(q)$. We use this as the measure of ideality [12].

Therefore, the real glass state does not have long-range order, and $\xi_s(T)$ describes the spatial extension of local DW order. The value of $\xi_s(T_g)$ reflects the consequence of the competition between the density wave and the SRO. The strength of the SRO depends on the nature of the atomic bonds. Metallic bonds are not directional, and are more compatible with the density waves, resulting in longer $\xi_s(T_g)$. Covalent bonds are directional, and are less compatible with the density waves, resulting in shorter $\xi_s(T_g)$. Indeed, $\xi_s(T_g)$ is closely related to liquid fragility [13], which reflects covalency [30].

This combined top-down/bottom-up approach makes it clear that the MRO is not a direct consequence of the SRO as has long been assumed, but it is a distinct property of liquid determined by the competition between the driving forces for the density waves and the SRO.

3.3. Topological MRO and MRO by Density Fluctuations

The term MRO is used also in describing the atomic structure just beyond the nearest neighbor atom shell [31–33]. It is a topological MRO, describing atom-atom correlation beyond the nearest neighbors. It is very difficult to detect it in the PDF, but it can be more clearly observed by fluctuation electron microscopy [34]. We consider it as an extension of the SRO [7,8,35], different from the MRO formed by density fluctuations discussed here which extends beyond the second peak of the PDF. As shown in Figure 3 the bulk of the second peak of the PDF is explained well as a part of the MRO oscillations by Equation (14). However, the split of the second peak of the PDF reflects the topological MRO [7,8]. Indeed, the position of the second peak in the PDF decreases as temperature is raised just as the first peak does [15,16], and the height of the second peak shows weaker freezing at T_g [17]. Thus, the second peak in the PDF reflects both the SRO (topological MRO) and the MRO by density waves. It represents the interface between the SRO and the MRO by density waves.

4. Changes in the SRO and MRO by Shear Stress

When a shear or uniaxial stress is applied to a glass the relative changes in atomic positions can be observed in terms of the anisotropic PDF expressed by the spherical harmonics expansion [36,37]. For affine (uniform) compressive uniaxial deformation the $l = 2, m = 0$ term is,

$$g_{2,affine}^0(r) = -\varepsilon \left(\frac{1}{5}\right)^{1/2} \frac{2(1+\nu)}{3} r \frac{d}{dr} g_0^0(r) \quad (15)$$

where ε is affine strain, ν is the Poisson's ratio and $g_0^0(r)$ is the isotropic PDF. In reality, the strain is not affine, so the anisotropic PDF can be expressed by

$$g_2^0(r) = -\varepsilon(r) \left(\frac{1}{5}\right)^{1/2} \frac{2(1+\nu)}{3} r \frac{d}{dr} g_0^0(r) \quad (16)$$

where the strain, $\varepsilon(r)$, is a function of distance. The macroscopic strain in metallic glasses is linear up to the elastic limit, so they are macroscopically elastic. At large distances the local strain becomes identical to the macroscopic strain, so that $\varepsilon(\infty)$ is equal to the macroscopic strain and $\varepsilon(r) - \varepsilon(\infty)$ describes the extent of deviation from affine deformation. Even though metallic glasses are macroscopically elastic up to the elastic limit, simulations suggest that at the atomic level, the nearest neighbor atoms show non-affine, non-elastic behavior [38].

As shown in Figure 4 [39] the part of the $\varepsilon(r)$ beyond the first peak (MRO) is constant at $\varepsilon(\infty)$, indicating elastic behavior. However, at the first peak (SRO) $\varepsilon(r)$ is appreciably below $\varepsilon(\infty)$, indicating that atomic rearrangements occur to relax local strain and deformation is not elastic in the nearest neighbor shell. This result is consistent with our observation that the MRO freezes at T_g , but the SRO does not and keeps increasing even below T_g [17]. In other words, a part of the atomic correlations expressed by the MRO behaves like an elastic body, but the immediate neighborhood of an atom described by the SRO is still partially liquid-like even in the glass state, and atoms are rearranged when stress is applied. This picture is consistent also with the theory of the glass transition [40], which assumes that about 20% of atoms are still liquid-like at the glass transition, and the glass transition occurs because of the loss of percolation of liquid-like atoms. On the other hand, when anelastic (creep) deformation occurs by applying stress at an elevated temperature below T_g , non-affine deformation occurs even for the MRO beyond the nearest neighbors as shown in Figure 4. This confirms the hypothesis that the macroscopic deformation is underpinned by the MRO.

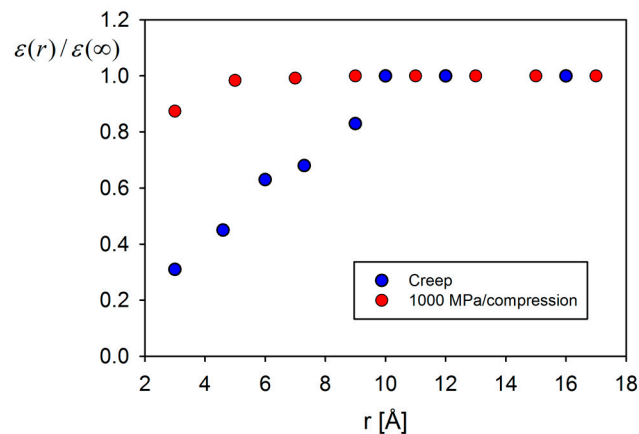


Figure 4. The r -dependent local strain determined from Equation (16) for the metallic glass sample under load of 1 GPa at room temperature (red) and for the sample anelastically creep deformed at 623 K under 1 GPa for 1 h (blue) [39].

5. Resistance to Deformation by MRO

The results shown in Figure 4 suggest that elasticity is maintained by the MRO, and not by the SRO. This statement, however, may sound preposterous. If the local environment cannot resist the applied stress, how can the whole body resist? The answers are the following:

- 1 Only less than 20% of atoms are liquid-like below T_g [40]. Because this is below the percolation limit, atomic rearrangements at the liquid-like sites remain local, and do not lead to macroscopic deformation.
- 2 The PDF first peak (SRO) and the peaks beyond (MRO) are different in nature [17–20]. The first peak describes the atom-atom correlation, whereas the MRO describes the atom-density correlation. The higher order peaks in the PDF include a large number of atoms. Thus, they describe coarse-grained density fluctuations rather than each atomic position. Therefore, the behavior of the MRO is closer to that of the bulk.

In the theory of the glass transition in metallic glasses [40] it was shown that the loss of percolation of liquid-like sites results in the glass transition. Here the liquid-like site is defined as atoms with the local atomic-level volume strain exceeding $\varepsilon_v^{T,crit} = \pm 0.11$ [40]. If the atomic-level volume strain, ε_v^T , exceeds $\varepsilon_v^{T,crit}$, the local coordination shell becomes unstable, because increasing or decreasing the coordination number becomes energetically preferred [41]. The ε_v^T has Gaussian distribution, and the atoms with $|\varepsilon_v^T|$ exceeding 0.11 are the liquid-like sites. Because the potential energy associated with the atomic-level volume fluctuations depend linearly on temperature [42], the standard deviation of ε_v^T is proportional to \sqrt{T} , and when the fraction of the liquid-like sites reaches the percolation limit the glass transition occurs. At the glass transition the atomic-level strains are frozen, so a glass below T_g retains liquid-like sites of which density is at the percolation limit, or about 20%. These sites will undergo local atomic rearrangement when stress is applied. But deformation remains local, because the density of the liquid-like sites is below the percolation limit.

Another evidence of locally liquid-like nature of metallic glass is found in the data for internal friction. Mechanical relaxation of glasses and liquids is characterized by at least two kinds of relaxation, the α -relaxation and the β -relaxation [43]. The α -relaxation describes the collective relaxation which leads to the glass transition, whereas the β -relaxation is due to local activation events and occurs even below T_g . In polymers the α -relaxation originates from the activation dynamics of main polymer chains, whereas the β -relaxation occurs due to the localized motion of side chains. In metallic glasses the α -relaxation describes the relaxation dynamics of the MRO [44]. The origin of the β -relaxation in metallic glasses is unclear, but it is most likely that it reflects short-range local cooperative atomic dynamics [45,46]. The β -relaxation in metallic glasses extend to low temperatures,

with the strength almost independent of temperature [47,48]. This also explains the strong temperature dependence of the shear modulus compared to that of the bulk modulus [49].

The magnitude of the non-affine deformation, the drop in $\varepsilon(r)$ at the first neighbor, $\Delta\varepsilon_R/\varepsilon_\infty = 1 - \varepsilon(r_1)/\varepsilon_\infty$, in Figure 4, is related to the ductility of the glass as shown in Figure 5 [50]. When it is larger than $\Delta\varepsilon_R/\varepsilon_\infty = 0.24$ the glass is ductile, whereas when it is less than 0.21 it is brittle. We found that this behavior is directly related to the strength of the MRO. As shown in Figure 6 the normalized MRO coherence length in the glass, $\zeta_s(T_g)/a$, is related to the plastic strain and the non-affine strain ratio ($\Delta\varepsilon_R/\varepsilon_\infty$). As we discussed above the value of $\zeta_s(T_g)/a$ reflects the competition between the density waves and the SRO. The results in Figure 6 show that a stronger MRO, thus a larger $\zeta_s(T_g)/a$, promotes ductility, and a stronger SRO, thus a smaller $\zeta_s(T_g)/a$, results in a brittle behavior. Because a strong SRO is a product of covalent bonding, this result is totally consistent with the intuition that covalency is responsible for brittleness. In Ref. [13] we showed that liquid fragility is linearly related to the number of atoms in the coherence volume, $n_s = 0 (\zeta_s)^3$. In Figure 6 $(\zeta_s/a)^3$, which is proportional to n_s , is compared to plastic strain and to $\Delta\varepsilon_R/\varepsilon_\infty$. Thus, when $(\zeta_s/a)^3$ is greater than 4.2, therefore when ζ_s/a is greater than 1.62, glasses are ductile, whereas when ζ_s/a is less than 1.62 they are brittle, although at present no theory explains this specific value. Thus, ductility is related also to fragility; fragile liquid produces ductile glass.

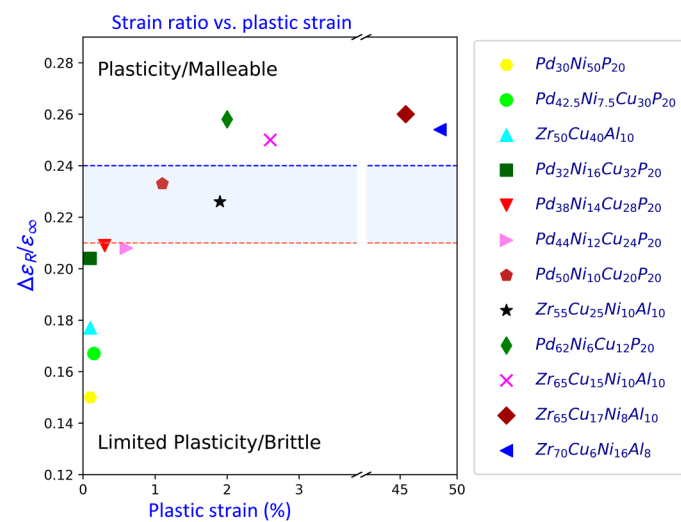


Figure 5. Metallic glasses with small non-affine strain ratio ($\Delta\varepsilon_R/\varepsilon_\infty$) are shown to have propensity to brittle fracture, whereas those with larger ratio are ductile [50].

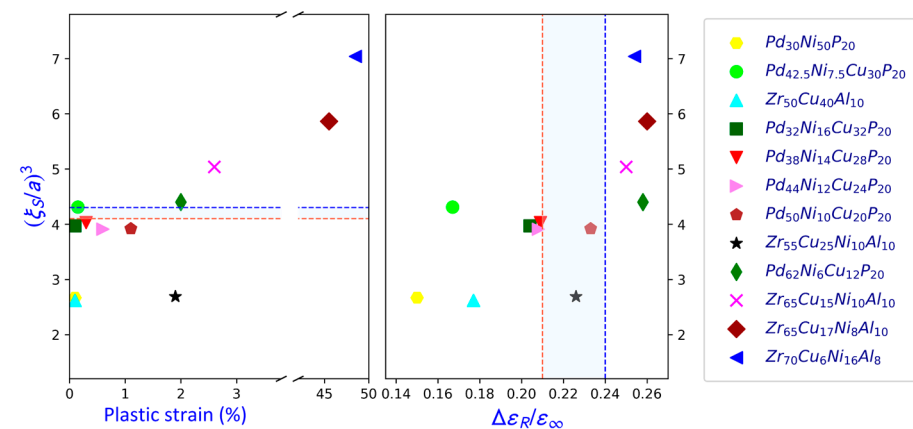


Figure 6. The normalized coherence volume, $(\zeta_s/a)^3$, against plastic strain (left) and the non-affine strain ratio, $\Delta\varepsilon_R/\varepsilon_\infty$ (right) for various metallic glasses.

Now, the ratio $\Delta\varepsilon_R/\varepsilon_\infty$ describes the extent of local strain relaxation in the nearest neighbor shell. Thus, we can write,

$$\Delta\varepsilon_R = \gamma_R \varepsilon_\infty p_R \quad (17)$$

where p_R is the density of relaxing atoms and γ_R is the local strain relaxation factor for each relaxation event. Note that $\gamma_R = 1$ if a single relaxation event fully relaxes the local atomic-level stress imposed by the applied stress, $\varepsilon_\infty = \sigma_a/G$, where σ_a is the applied stress and G is the shear modulus. As p_R it is reasonable to assume that it is the density of liquid-like sites, $p_R = 0.24$ [40]. Interestingly, the critical value of the non-affine strain ratio is $\Delta\varepsilon_R/\varepsilon_\infty = 0.24$. This means $\gamma_R = 1$ at the critical condition for ductile/brittle transition. In other words, a glass is ductile when $\gamma_R > 1$, and a relaxation event relaxes the stress beyond the nearest neighbor shell. This will cause relaxation on the neighbor atoms and start a cascade action of local relaxation on more than one atom. That is exactly the mechanism of ductile flow suggested by simulation [51].

These results show that when the shear stress below the yield stress is applied to metallic glass atoms in the nearest neighbor shell become rearranged and the stress is relaxed, but the MRO behaves elastically without relaxation. Therefore, applied shear stress is resisted by the MRO, not the SRO, and macroscopic mechanical deformation is controlled by the cooperative MRO represented by local density waves. A solid-like behavior of glass is usually explained in terms of atomic caging [42]. For a long time, caging has been thought to occur due to the tightened shell of the nearest neighbor atoms [43,52], but the new results discussed here suggest that the caging is achieved by the MRO, not by the SRO. The immediate atomic environment, SRO, still retains partially liquid-like in nature. However, the liquid-like sites do not percolate [37,39], resulting in a rigid MRO which provides resistance to deformation.

6. Defects vs. Bulk

Crystalline solids mechanically fail through the motion of defects, such as dislocations. In association there have been extensive efforts to find defects in metallic glasses as a mechanism of plastic deformation [53–58]. However, our results discussed above suggest that mechanical deformation in metallic glasses is controlled by the MRO, which is a bulk property, in thermal equilibrium in the liquid just above T_g [28]. How can these opposing approaches be reconciled? Our view is that defect may locally start deformation, but the ultimate resistance is provided by the MRO.

In crystalline solids defects maintain their identities after motion, because they are topologically protected by lattice periodicity. But in glasses they are not, and their structure changes quite substantially upon movement because of extensive atomic rearrangements. In fact, by going through the saddle point of the potential energy landscape (PEL) the system loses thermal memory [59] because the local structure topologically melts [60]. It is well known in mathematics that the saddle point is a generator of chaos [61,62]. Thus, deformation may start from local defective sites, but by the time it reaches the saddle point it does not matter where it came from. The overall resistance is determined by the average structure represented by the MRO.

Conversely, focusing on particular local topology, such as icosahedral clusters, as a mechanism of structural stability may be misguided, because the MRO represents coarse grained density fluctuations, independent of details of the local structure. The variations in the local structure are controlled by the distribution in the volume strain frozen in at the glass transition [28,40]. Formation of icosahedron, which has relatively small atomic-level volume strain, is just a consequence of such distributions. Specific topologies of the local structure depend on composition through relative atomic sizes and the nature of atomic bonding, and they are almost irrelevant to the stability of the average structure.

It is interesting to note that a recent work [63] to model glasses with cooling rates comparable to those by experiments, achieved by a combination of molecular dynamics (MD) and Monte-Carlo (MC) simulation, suggests that much of the low-density defects

observed by many MD simulations are likely to be artifacts of unrealistically high cooling rates in the simulation. According to Ref. [63] in real glass the region of cooperativity [64] is much smaller in size than previously assumed, involving only about 10 atoms. This size is close to those of bulk simulation and theory without assuming defects, which are about 5 atoms [65,66]. Our view is that deformation of metallic glasses at the atomic level is controlled not by defective weak spots as is usually assumed, but by the strong resistance due to the MRO. If the strength is controlled by defects, it should show strong structure-sensitivity as in crystalline solids. However, the strength of metallic glasses is universally dependent only on elastic modulus and is rather insensitive to structural details [67,68]. This observation strongly supports our view that the bulk properties, such as the MRO, rather than defects, control mechanical properties of metallic glasses.

7. Conclusions

The conventional view on the stability of the glass structure and its mechanical response has been to focus on local structure of the nearest neighbors, particularly on well-ordered structures, such as icosahedral clusters, and consider them as the building blocks to construct the structure. However, the local structures vary with composition and chemistry, and this bottom-up approach does not lead to a holistic general view on the structure. Instead, we focused on the MRO which appears quite generally and persistently. Traditionally the MRO has been regarded as a direct consequence of the SRO [14]. However, the SRO and the MRO are fundamentally different in nature [18,38] and behave differently with temperature [15–17]. In our top-down approach with the density wave theory the MRO is a product of compromise between the density wave and the SRO. The MRO provides the main resistance to deformation, whereas the SRO is partially liquid-like and does not offer overall resistance. We have to conclude that, unlike in crystalline solids, largely mechanical properties of metallic glasses are controlled not by structural defects, but by the MRO.

Author Contributions: Conceptualization, T.E.; data curation, W.D. and C.W.R.; writing—original draft preparation, T.E.; writing—review and editing, W.D. and C.W.R. All authors have read and agreed to the published version of the manuscript.

Funding: This work was supported by the U.S. Department of Energy, Office of Science, Basic Energy Science, Materials Sciences and Engineering Division.

Informed Consent Statement: Not applicable.

Data Availability Statement: Original data are available upon request to the contact person.

Conflicts of Interest: The authors declare no conflict of interest.

References

1. Egelstaff, P.A. *An Introduction to the Liquid State*, 1st ed.; Academic Press: Cambridge, MA, USA, 1967.
2. Croxton, C.A. *Liquid State Physics—A Statistical Mechanical Introduction*; Cambridge University Press: Cambridge, UK, 1974.
3. Hansen, J.-P.; McDonald, I.R. *Theory of Simple Liquids*; Academic Press: London, UK, 1976; Volume 1986, p. 2006.
4. Bernal, J.D. A geometrical approach to the structure of liquids. *Nature* **1959**, *183*, 141–147. [[CrossRef](#)]
5. Nelson, D.R. Order, frustration, and defects in liquids and glasses. *Phys. Rev. B* **1983**, *28*, 5515–5535. [[CrossRef](#)]
6. Miracle, D.B. A structural model for metallic glasses. *Nat. Mater.* **2004**, *3*, 697–702. [[CrossRef](#)]
7. Sheng, H.W.; Luo, W.K.; Alamgir, F.M.; Bai, J.M.; Ma, E. Atomic packing and short-to-medium-range order in metallic glasses. *Nature* **2006**, *439*, 419–425. [[CrossRef](#)] [[PubMed](#)]
8. Din, J.; Ma, E.; Asta, M.; Ritchie, R.O. Second-nearest-neighbor correlations from connection of atomic packing motifs in metallic glasses and liquids. *Sci. Rep.* **2015**, *5*, 17429.
9. Cargill, G.S., III. Structure of metallic alloy glasses. *Solid State Phys.* **1975**, *30*, 227–320.
10. Voylov, D.N.; Griffin, P.J.; Mercado, B.; Keum, J.K.; Nakanishi, M.; Novikov, V.N.; Sokolov, A.P. Correlation between temperature variations of static and dynamic properties in glass-forming liquids. *Phys. Rev. E* **2016**, *94*, 060603. [[CrossRef](#)]
11. Ryu, C.W.; Dmowski, W.; Kelton, K.F.; Lee, G.W.; Park, E.S.; Morris, J.R.; Egami, T. Curie-Weiss behavior of liquid structure and ideal glass state. *Sci. Rep.* **2019**, *9*, 18579. [[CrossRef](#)]
12. Ryu, C.W.; Dmowski, W.; Egami, T. Ideality of Liquid Structure: A Case Study for Metallic Alloy Liquids. *Phys. Rev. E* **2020**, *101*, 030601. [[CrossRef](#)]

13. Ryu, C.W.; Egami, T. Origin of liquid fragility. *Phys. Rev. E* **2020**, *102*, 042615. [[CrossRef](#)]
14. Ornstein, L.S.; Zernike, F. Accidental deviations of density and opalescence at the critical point of a single substance. *Roy. Neth. Acad. Arts Sci. (KNAW)* **1914**, *17*, 793–806.
15. Lou, H.; Wang, X.; Cao, Q.; Zhang, D.; Zhang, J.; Hu, T.; Mao, H.; Jiang, J.-Z. Negative expansions of interatomic distances in metallic melts. *Proc. Nat. Acad. Sci. USA* **2013**, *110*, 10068. [[CrossRef](#)]
16. Wei, S.; Stolpe, M.; Gross, O.; Evenson, Z.; Gallino, I.; Hembree, W.; Bednarcik, J.; Kruzic, J.J.; Busch, R. Linking structure to fragility in bulk metallic glass-forming liquids. *Appl. Phys. Lett.* **2015**, *106*, 181901. [[CrossRef](#)]
17. Ryu, C.W.; Egami, T. Medium-range atomic correlation in simple liquid. I. Distinction from short-range order. *Phys. Rev. E* **2021**, *104*, 064109. [[CrossRef](#)] [[PubMed](#)]
18. Egami, T. Local density correlations in liquids. *Front. Phys.* **2020**, *8*, 50. [[CrossRef](#)]
19. Egami, T.; Ryu, C.W. Structural principles in metallic liquids and glasses: Bottom-up or top-down. *Front. Mater.* **2022**, *9*, 874191. [[CrossRef](#)]
20. Egami, T.; Ryu, C.W. Medium-range atomic correlation in simple liquid. III. Density wave theory. *arXiv* **2022**, arXiv:2211.07702.
21. Goldstein, M. Viscous liquids and the glass transition: A potential energy barrier picture. *J. Chem. Phys.* **1969**, *51*, 3728–3739. [[CrossRef](#)]
22. Debenedetti, P.G.; Stillinger, F.H. Supercooled liquids and the glass transition. *Nature* **2001**, *410*, 259–267. [[CrossRef](#)]
23. Rowley, L.A.; Nicholson, D.; Parsonage, N.G. Monte Carlo grand canonical ensemble calculation in a gas-liquid transition region for 12-6 Argon. *J. Comp. Phys.* **1975**, *17*, 401–414. [[CrossRef](#)]
24. Warren, B.E. *X-ray Diffraction*; Addison-Wesley, Reading: Boston, MA, USA, 1969.
25. Egami, T.; Ryu, C.W. World beyond the nearest neighbors. *J. Phys. Cond. Mat.* **2023**, *in press*.
26. Shechtman, D.; Blech, I.; Gratias, D.; Cahn, J.W. Metallic phase with long-range orientational order and no translational symmetry. *Phys. Rev. Lett.* **1984**, *53*, 1951–1954. [[CrossRef](#)]
27. Levine, D.; Steinhardt, P.J. Quasicrystals: A new class of ordered structures. *Phys. Rev. Lett.* **1984**, *53*, 2477–2480. [[CrossRef](#)]
28. Egami, T.; Ryu, C.W. Medium-range atomic correlation in simple liquid. II. Theory of temperature dependence. *Phys. Rev. E* **2021**, *104*, 064110. [[CrossRef](#)]
29. McGreevy, R.L. Reverse Monte Carlo modelling. *J. Phys. Condens. Matter* **2001**, *13*, R877–R913. [[CrossRef](#)]
30. Angell, C.A. Formation of glasses from liquids and biopolymers. *Science* **1995**, *267*, 1924–1935. [[CrossRef](#)]
31. Zhang, P.; Wang, Z.; Perepezko, J.H.; Voyles, P.M. Vitrification, crystallization, and atomic structure of deformed and quenched Ni₆₀Nb₄₀ metallic glass. *J. Non-Cryst. Solids* **2018**, *491*, 133–140. [[CrossRef](#)]
32. Davani, F.A.; Hilke, S.; Rösner, H.; Geissler, D.; Gebert, A.; Wilde, G. Correlations between the ductility and medium-range order of bulk metallic glasses. *J. Appl. Phys.* **2020**, *128*, 015103. [[CrossRef](#)]
33. Im, S.; Wang, Y.; Zhao, P.; Yoo, G.H.; Chen, Z.; Calderon, G.; Gharacheh, M.A.; Zhu, M.; Licata, O.; Mazumder, B.; et al. Medium-range ordering, structural heterogeneity, and their influence on properties of Zr-Cu-Co-Al metallic glasses. *Phys. Rev. Res.* **2021**, *5*, 115604. [[CrossRef](#)]
34. Gibson, J.M.; Treacy, M.M.J.; Voyles, P.M. Atom pair persistence in disordered materials from fluctuation microscopy. *Ultramicroscopy* **2000**, *83*, 169–178. [[CrossRef](#)]
35. Cheng, Y.Q.; Ma, E.; Sheng, H.W. Atomic level structure in multicomponent bulk metallic glass. *Phys. Rev. Lett.* **2009**, *102*, 245501. [[CrossRef](#)]
36. Egami, T.; Billinge, S.J.L. *Underneath the Bragg Peaks: Structural Analysis of Complex Materials*, 1st ed.; Pergamon Press: Oxford, UK, 2003.
37. Suzuki, Y.; Haimovich, J.; Egami, T. Bond-orientational anisotropy in metallic glasses observed by x-ray diffraction. *Phys. Rev. B* **1987**, *35*, 2162–2168. [[CrossRef](#)] [[PubMed](#)]
38. Suzuki, Y.; Egami, T. Shear deformation of glassy metals: Breakdown of Cauchy relationship and anelasticity. *J. Non-Cryst. Solids* **1985**, *75*, 361–366. [[CrossRef](#)]
39. Egami, T.; Iwashita, T.; Dmowski, W. Mechanical properties of metallic glasses. *Metals* **2013**, *3*, 77–113. [[CrossRef](#)]
40. Egami, T.; Poon, S.J.; Zhang, Z.; Keppens, V. Glass transition in metallic glasses: A microscopic model of topological fluctuations in the bonding network. *Phys. Rev. B* **2007**, *76*, 024203. [[CrossRef](#)]
41. Egami, T. Atomic level stresses. *Progr. Mater. Sci.* **2011**, *56*, 637–653. [[CrossRef](#)]
42. Chen, S.P.; Egami, T.; Vitek, V. Local fluctuations and ordering in liquid and amorphous metals. *Phys. Rev. B* **1988**, *37*, 2440–2449. [[CrossRef](#)] [[PubMed](#)]
43. Donth, E. *The Glass Transition: Relaxation Dynamics of Liquids and Disordered Materials*; Springer: Berlin, Germany, 2010.
44. Ryu, C.W.; Egami, T. Medium-Range Atomic Correlation in Simple Liquids. IV. Alpha-Relaxation by Scattering. 2023, unpublished article.
45. Wang, W.H. Dynamic relaxations and relaxation-property relationships in metallic glasses. *Prog. Mater. Sci.* **2019**, *106*, 100561. [[CrossRef](#)]
46. Yu, H.-B.; Richert, R.; Samwer, K. Structural rearrangements governing Johari-Goldstein relaxations in metallic glasses. *Sci. Adv.* **2017**, *3*, e1701577. [[CrossRef](#)]
47. Jiang, H.Y.; Luo, P.; Wen, P.; Bai, H.Y.; Wang, W.H.; Pan, M.X. The near constant loss dynamic mode in metallic glass. *J. Appl. Phys.* **2016**, *120*, 145106. [[CrossRef](#)]

48. Zella, L.; Moon, J.; Keffer, D.; Egami, T. Transient nature of fast relaxation in metallic glass. *Acta Mater.* **2022**, *239*, 118254. [[CrossRef](#)]
49. Zhang, Z.; Keppens, V.; Egami, T. A simple model to predict the temperature dependence of elastic moduli of bulk metallic glasses. *J. Appl. Phys.* **2007**, *102*, 123508. [[CrossRef](#)]
50. Wang, H.; Dmowski, W.; Wang, Z.; Tong, Y.; Yokoyama, Y.; Ketkaew, J.; Schroers, J.; Egami, T. Non-affine strains control ductility of metallic glasses. *Phys. Rev. Lett.* **2022**, *128*, 155501. [[CrossRef](#)] [[PubMed](#)]
51. Fan, Y.; Iwashita, T.; Egami, T. Crossover from localized to cascade relaxations in metallic glasses. *Phys. Rev. Lett.* **2015**, *115*, 045501. [[CrossRef](#)]
52. Kleban, P. Toward a microscopic basis for the de Gennes narrowing. *J. Stat. Phys.* **1974**, *11*, 317–322. [[CrossRef](#)]
53. Spaepen, F. A microscopic mechanism for steady state inhomogeneous flow in metallic glasses. *Acta Metall.* **1977**, *25*, 407–415. [[CrossRef](#)]
54. Argon, A.S. Plastic deformation in metallic glasses. *Acta Metall.* **1979**, *27*, 47–58. [[CrossRef](#)]
55. Srolovitz, D.; Maeda, K.; Vitek, V.; Egami, T. Structural defects in amorphous solids: Statistical analysis of a computer model. *Philos. Mag. A* **1981**, *44*, 847–866. [[CrossRef](#)]
56. Falk, M.L.; Langer, J.S. Dynamics of viscoplastic deformation in amorphous solids. *Phys. Rev. E* **1998**, *57*, 7192–7205. [[CrossRef](#)]
57. Cubuk, E.D.; Schoenholz, S.S.; Rieser, J.M.; Malone, B.D.; Rottler, J.; Durian, D.J.; Kaxiras, E.; Liu, A.J. Identifying structural flow defects in disordered solids using machine-learning methods. *Phys. Rev. Lett.* **2015**, *114*, 108001. [[CrossRef](#)]
58. Bapst, V.; Keck, T.; Grabska-Barwińska, A.; Donner, C.; Cubuk, E.D.; Schoenholz, S.S.; Obika, A.; Nelson, A.W.R.; Back, T.; Hassabis, D.; et al. Unveiling the predictive power of static structure in glassy systems. *Nat. Phys.* **2020**, *16*, 448–454. [[CrossRef](#)]
59. Fan, Y.; Iwashita, T.; Egami, T. Energy landscape-driven nonequilibrium evolution of inherent structure in disordered material. *Nat. Commun.* **2017**, *8*, 15417. [[CrossRef](#)] [[PubMed](#)]
60. Ding, J.; Li, L.; Wang, N.; Tian, L.; Asta, M.; Ritchie, R.O.; Egami, T. Universal nature of the saddle states of structural excitations in metallic glasses. *Mater. Today Phys.* **2021**, *17*, 100359. [[CrossRef](#)]
61. Mason, J.F.; Piironen, P.T. Saddle-point solutions and grazing bifurcations in an impacting system. *Chaos* **2012**, *22*, 013106. [[CrossRef](#)]
62. Párraga, H.; Arranz, F.J.; Benito, R.M.; Borondo, F. Above saddle-point regions of order in a sea of chaos in the vibrational dynamics of KCl. *J. Phys. Chem. A* **2018**, *122*, 3433–3441. [[CrossRef](#)]
63. Zhang, Z.; Ding, J.; Ma, E. Shear transformations in metallic glasses without excessive and predefinable defects. *Proc. Nat. Acad. Sci. USA* **2022**, *119*, e2213941119. [[CrossRef](#)] [[PubMed](#)]
64. Adam, G.; Gibbs, J.H. On the temperature dependence of cooperative relaxation properties in glass forming liquids. *J. Chem. Phys.* **1965**, *43*, 139–146. [[CrossRef](#)]
65. Fan, Y.; Iwashita, T.; Egami, T. How thermally induced deformation starts in metallic glass. *Nat. Commun.* **2014**, *5*, 5083. [[CrossRef](#)] [[PubMed](#)]
66. Bellissard, J. Delone Sets and Material Science: A Program, in Mathematics of Aperiodic Order. In *Progress in Mathematics*; Kellerdonk, J., Lenz, D., Savinien, J., Eds.; Birkhauser Verlag: Basel, Switzerland, 2015; Volume 309, pp. 405–428.
67. Johnson, W.L.; Samwer, K. A universal criterion for plastic yielding of metallic glasses with a $(T/T_g)^{2/3}$ temperature dependence. *Phys. Rev. Lett.* **2005**, *95*, 195501. [[CrossRef](#)]
68. Wang, W.H. Elastic moduli and behaviors of metallic glasses. *J. Non-Cryst. Solids* **2005**, *351*, 1481–1485. [[CrossRef](#)]

Disclaimer/Publisher’s Note: The statements, opinions and data contained in all publications are solely those of the individual author(s) and contributor(s) and not of MDPI and/or the editor(s). MDPI and/or the editor(s) disclaim responsibility for any injury to people or property resulting from any ideas, methods, instructions or products referred to in the content.